The Performance Improvement of Ultrasound Localization Microscopy (ULM) Using the Robust Principal Component Analysis (RPCA)

Duong-Hung Pham, Vassili Pustovalov, Denis Kouamé

The Performance Improvement of Ultrasound Localization Microscopy (ULM) Using the Robust Principal Component Analysis (RPCA)

Duong Hung Pham, Vassili Pustovalov and Denis Kouamé

***Abstract*— This paper presents an algorithm for ultrafast ultrasound localization microscopy (ULM) used for the detection, localization, accumulation, and rendering of intravenously injected ultrasound contrast agents (UCAs) enabling to yield hemodynamic maps of the brain microvasculature. It consists in integrating a robust principal component analysis (RPCA)-based approach into the ULM process for more robust tissue filtering, resulting in more accurate ULM images. Numerical experiments conducted on an *in vivo* rat brain perfusion dataset demonstrate the efficiency of the proposed approach compared to the most widely used state-of-the-art method.**

***Index Terms*— ULM, ultrafast ultrasound, inverse problems, robust PCA, blood flow, tissue filtering, UCA localization.**

I. INTRODUCTION

Ultrasound (US) imaging is increasingly used in medical practice as a non-invasive, nonionizing radiation, low-cost, and ease-of-use tool. Using plane wave techniques, the US modality can perform acquisitions with a frame rate up to 20kHz, which enables a good visualization and quantification of microvascular structure including sudden functional changes in the brain, as well as an increase of blood-low sensitivity for more accurate filtering [1]. However, the propagation of US waves faces many phenomena including diffraction and attenuation, resulting in a limited spatial resolution. The recent advent of ultrasound localization microscopy (ULM) successfully handles the trade-off of US imaging between spatial resolution and penetration depth while achieving a high sensitivity thanks to the clever interaction between sparse ultrasound contrast agents (UCAs) and ultrafast imaging [2]. Having a similar principle to photoactivated localization microscopy (PALM), ULM considers UCAs as sensors to image the region of interest by detecting, localizing, accumulating, and rendering thousands of microbubble events through density-based techniques. Besides, the high framerate within ULM allows the retrieval of the trajectories of UCAs in the bloodstream, thus imaging efficiently both the vasculature and microvasculature. Interestingly, ULM has been freshly adapted for 2D transcranial application, which has the potential of providing new imaging biomarkers for early detection, diagnosis, and prognosis of many cerebral diseases [3]. Despite its efficiency, most current algorithms for ULM have been implemented together with a *trivial* spatio–temporal singular value decomposition (SVD) filter [3]–[5]. The idea of using this technique emanates from the fact that in US imaging, particularly ultrafast technique, back-scattered blood signals carrying UCAs (originating from vessels) and clutter signals (from tissues surrounding the vessels) superimpose themselves on the images [6]. Applying tissue filtering consequently enables the removal of unwanted clutter signals from stationary or moving tissues to retain only the contribution of individual UCAs. The SVD technique is fast and straightforward; however, the empirical tuning process of its thresholding parameters does not rely on any interpretable model, which remains problematic in practice, limiting the method's applicability.

In this paper, we propose to use an alternative technique for tissue filtering, namely a robust principal component analysis (RPCA), resulting in more accurate and saturated ULM images [7]. The principle of RPCA is to formulate tissue filtering as an inverse problem of the blood-tissue separation, where *a priori* knowledge about tissue and blood structures carrying UCAs can be incorporated. In practice, the tissues are assumed to be low-rank while the blood flow is sparse. The inverse problem is then solved using iterative approaches such as the alternating direction method of multipliers (ADMM) [8]. The remainder of the paper is organized as follows. The background about SVD-based ULM is given in Section II. The proposed PRCA-based ULM algorithm is detailed in Section III. Finally, numerical results on *in vivo* ultrafast US data are regrouped in Section IV, showing the improvement achieved by the proposed approach over the most efficient algorithm for ULM nowadays.

II. BACKGROUND ON SVD-BASED ULM

Ultrasound localization microscopy (ULM) is a multi-step process including six main steps resumed as follows[1]. 1) Acquisition of raw US images of a perfused organ injected with UCAs at a high frame rate. 2) Tissue filtering on these images to get rid of tissue signals. 3) Detection and localization of UCAs with sub-pixel precision. 4) Pairing successive positions of the detected UCAs together into tracks. 5) Interpolation and projection of the tracks on a rendering grid. 6) Reconstruction of ULM vascular image accumulating a large number of tracks (called rendering). The quality of ULM images is strongly dependent upon all the steps above which have been greatly improved over the past decade. For instance, a thorough study of ULM framework has been introduced including 6 sets of *in vitro* and *in vivo* data and a systematic comparison of the seven most used algorithms for UCAs localization in [5]. In this

D. H. Pham, V. Pustovalov and D. Kouamé are with the IRIT Lab, Université de Toulouse, and CNRS UMR 5505, 31400 Toulouse, France. Email: {duong-hung.pham; vassili.pustovalov; denis.kouame}@irit.fr.

[1]The interested reader is referred to [5] for a detailed description of these steps of the method.

article, we focus on the improvement of the tissue filtering step which is often overlooked in previous works [3]–[5]. Indeed, in these works, a *trivial* SVD was used to separate blood flow containing UCAs from unwanted tissue signals, and also to increase the Doppler sensitivity of the resulting image. It consists in factorizing the 2D Casorati matrix $\boldsymbol{S} \in \mathbb{C}^{N_z N_x \times N_t}$ (i.e. obtained by stacking the frames into columns of the recorded image) using SVD as follows [6]:

$$\boldsymbol{S} = \boldsymbol{U}\boldsymbol{\Sigma}\boldsymbol{V}^{\dagger} = \sum_{k=1}^{r} \boldsymbol{u}_k \sigma_k \boldsymbol{v}_k^{\dagger}, \tag{1}$$

where N_z, N_x, and N_t are respectively the axial, lateral, and temporal dimensions. $\boldsymbol{U} \in \mathbb{C}^{N_z N_x \times N_z N_x}$ and $\boldsymbol{V} \in \mathbb{C}^{N_t \times N_t}$ are two unitary matrices of the spatial (left) $\boldsymbol{u}_k$ and temporal (right) $\boldsymbol{v}_k$ singular vectors. $\boldsymbol{\Sigma} \in \mathbb{R}^{N_z N_x \times N_t}$ is a non-square diagonal matrix with diagonal elements being its singular values σ_k. $\dagger$ denotes the conjugate transpose and $r = \min(N_z N_x, N_t)$ the rank of $\boldsymbol{S}$. It is worth mentioning that the diagonal elements $\boldsymbol{\Sigma}$ are sorted in ascending order of magnitude. The smallest singular values correspond to the noises, the intermediate ones to the blood signals, and the largest ones to the tissue signals. Then, some empirical heuristics are used to tune the clutter T_c and blood T_b thresholds. This enables to filter out the unwanted tissue signals and the noises, and also to reveal of the blood flow components as follows:

$$\hat{\boldsymbol{B}} = \sum_{k=T_c}^{T_b} \boldsymbol{u}_k \sigma_k \boldsymbol{v}_k^{\dagger}. \tag{2}$$

Although the SVD technique is very simple and can perform at a very low computational cost, the manual choice of the optimal thresholds is not obvious, not only in the ULM scenario but also in other practical situations, thus making its applicability complex.

III. PROPOSED RPCA-BASED ULM

The main aim of the proposed algorithm is to enhance the ultimate ULM image quality by integrating a more efficient tissue filtering technique in the ULM process in the place of SVD. To this end, we investigate a robust principal component analysis (RPCA)-based technique [7] as an alternative solution. It consists in formulating blood-tissue separation as an inverse problem, where *a priori* knowledge about tissue and blood structures with UCAs is taken into account. The blood flow with UCAs $\boldsymbol{B}$ is assumed to be sparse and is conventionally promoted by the minimization of the l_1-norm. The tissue signals $\boldsymbol{T}$ is assumed to change very slowly with time, leading to a low-ranking assumption on $\boldsymbol{T}$ which is usually modeled by the nuclear norm $||.||_*$. $\boldsymbol{N}$ is assumed to be a Gaussian noise. Thus, RPCA is expressed as the following convex optimization problem:

$$[\hat{\boldsymbol{B}}, \hat{\boldsymbol{T}}] = \arg\min_{\boldsymbol{B},\boldsymbol{T}} \left\{ ||\boldsymbol{S} - \boldsymbol{B} - \boldsymbol{T}||_F^2 + \lambda ||\boldsymbol{B}||_1 + \rho ||\boldsymbol{T}||_* \right\}, \tag{3}$$

where $\hat{.}$ stands for the estimated variables, $||.||_F$ is the Frobenius norm, and $\lambda, \rho > 0$ are two hyperparameters balancing the trade-off between the blood sparsity and the tissues' low-rankness [9]. To solve (3), the augmented Lagrangian-based alternating direction method of multipliers (ADMM) is used. It consists in solving iteratively several sub-problems over each variable separately [8]. Precisely, the augmented Lagrangian related to (3) is first written as follows:

$$\mathscr{L}(\boldsymbol{B}, \boldsymbol{T}, \boldsymbol{\nu}) = \lambda ||\boldsymbol{B}||_1 + \rho ||\boldsymbol{T}||_* + \frac{\mu}{2} ||\boldsymbol{S} - \boldsymbol{B} - \boldsymbol{T} + \frac{1}{\mu}\boldsymbol{\nu}||_F^2,$$

where $\boldsymbol{\nu}$ is the Lagrange multiplier and μ is the Lagrangian penalty parameter controlling the convergence speed of the algorithm. Finally, at each iteration k, ADMM performs the following three steps, until a predefined *stopping* criteria is met:

$$\hat{\boldsymbol{B}}^{(k+1)} = \arg\min_{\boldsymbol{B}} (\lambda ||\boldsymbol{B}||_1 + \frac{\mu}{2} ||\boldsymbol{B} - (\boldsymbol{S} - \boldsymbol{T}^{(k)} + \frac{1}{\mu}\boldsymbol{\nu}^{(k)})||_F^2)$$

$$\hat{\boldsymbol{T}}^{(k+1)} = \arg\min_{\boldsymbol{T}} (\rho ||\boldsymbol{T}||_* + \frac{\mu}{2} ||\boldsymbol{T} - (\boldsymbol{S} - \boldsymbol{B}^{(k+1)} + \frac{1}{\mu}\boldsymbol{\nu}^{(k)})||_F^2)$$

$$\boldsymbol{\nu}^{(k+1)} = \boldsymbol{\nu}^{k} + \mu(\boldsymbol{S} - \boldsymbol{B}^{(k+1)} - \boldsymbol{T}^{(k+1)}).$$

It is interesting to note that the two first steps for $\hat{\boldsymbol{B}}^{(k+1)}$ and $\hat{\boldsymbol{T}}^{(k+1)}$ are both convex problems associated, respectively, with closed-form solutions: soft thresholding (ST) [10] and singular value thresholding (SVT) [11]. Note that other RPCA-related approaches, *e.g.* [12], [13] can also be used.

IV. NUMERICAL RESULTS

This section regroups numerical results on a *in vivo* rat brain perfusion dataset to illustrate the improvement brought by the proposed algorithm over the most efficient method currently for ULM. Note that due to space limitation, only this *in-vivo* data will be used to illustrate the proposed approach. As mentioned above, an exhaustive study conducted in [5] drew a conclusion that SVD-based UML with radial symmetry (RS) algorithm for UCAs localization came out on top both in qualitative and quantitative evaluations. Therefore, it will be selected for comparison with our proposed algorithm in the sequel.

A. In vivo rat brain perfusion dataset

This dataset is the *in vivo* angiography of the rat brain that is publicly available at [15]. Before the acquisition, the skull of the rat had been removed following a craniotomy surgery protocol. Then, UCAs ($400\mu l$, Bracco Imaging, Italy) were continuously injected through the jugular vein ($192,000$ US images). The radiofrequency data were beamformed on the ultrasound machine's graphics processing unit (SuperSonic Imagine). An US acquisition comprising of 240 blocs of 800 frames of size 78x118 pixels was taken at a compounded frame rate of 1KHz with 3 tilted plane waves $[-3^{\text{o}}, 0^{\text{o}}, +3^{\text{o}}]$ and pulse repetition frequency 15 MHz (Vermon, France) with a 0.1mm pitch. The acquisition time was 4 min. Refer to [5] for more details.

B. Performance comparison

The hyperparameters of the two studied algorithms were tuned to maximize the performance measures. To this end, those of SVD-based ULM were kept the same as in the original publication, which showed the best performance [5].

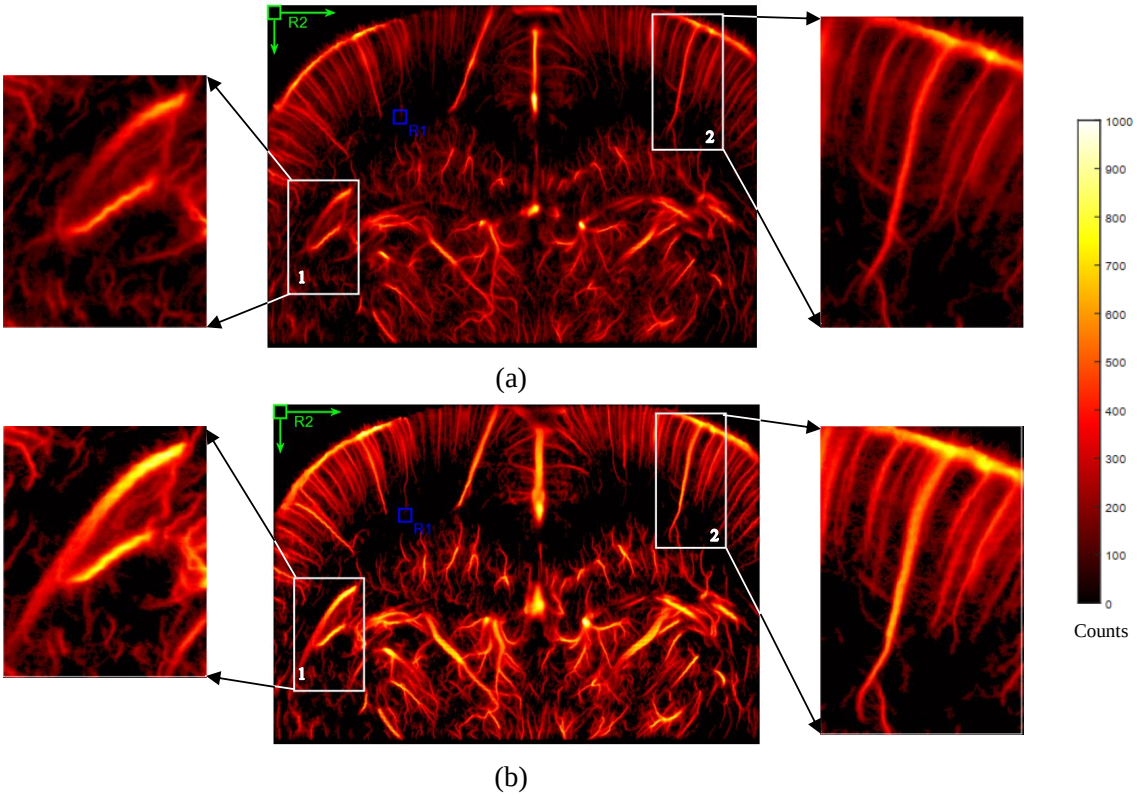

Fig. 1. ULM density-based rendering images of *in vivo rat brain perfusion* with two zoomed-in regions: 1 (*left panel*) and 2 (*right panel*). The density renderings are obtained by counting the number of UCAs trajectories passing each pixel in the image (unit: counts). The density rendering using the RS localization algorithm. Composite rendering of 192,000 frames. (a) the SVD-based ULM; (b) the proposed PRCA-based ULM. All images are displayed with a dynamic range of 1000 counts, and the zoomed-in boxes show the same magnified areas in each image.

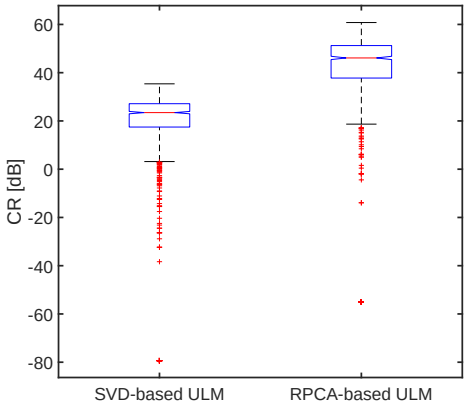

Fig. 2. CR measures for the two tested methods. In these boxplots, the red horizontal line indicates the median, the bottom and top edges of the box indicate the 25th and 75th percentiles and the black lines indicate the entire range of data samples, per category. Red markers indicate outliers excluded from the statistical calculations [14]. For this simulation, the median of the SVD-based ULM is 23.45 whereas the one of the proposed PRCA-based ULM is 46.11.)

Particularly, the SVD relying on two distinct thresholds to filter the eigenvalues were, respectively, chosen as $T_c = 5$ and $T_b = 800$. For the RPCA-based ULM, we recall that λ and ρ associated with RPCA express the compromise between the blood sparsity and the tissue low-rankness while μ manages the convergence speed of the algorithm. As suggested in [9] for the general RPCA problem, ρ was set to 1 while the reference values $\lambda_{\text{ref}} = \frac{1}{\sqrt{\max(Nz \times Nx, Nt)}}$ and $\mu_{\text{ref}} = 10 \times \lambda_{\text{ref}}$, were applied to ease the tuning. With this in mind, the best values of λ and μ selected were respectively set to 0.0104 and 0.104, in the experiments. Note also that the RS algorithm for UCAs localization with the same parameter setting for both two studied algorithms was used to ensure a fair comparison.

In Fig. 1, we depict the ULM density rendering images along with two zoomed-in regions obtained by the two algorithms carried out on the *in vivo* rat brain perfusion dataset. The density rendering image shows the number of trajectories passing through a single pixel whose square size is set to $10\mu m \times 10\mu m$. Visually judging these plots, one may notice that the proposed RPCA-based ULM algorithm yields a density rendering image that is overall less noisy and more saturated vessels than the SVD-based ULM one. Looking at the two zoomed-in regions, one may further remark that the delineation of blood vessels given by the proposed method is sharper and more accurate.

In order to compare the performance of the two studied algorithms on the *in-vivo* data, two commonly employed quantitative measures are used. The first one is the resolution gain (RG) as suggested in [16]. It is defined as a ratio between the number of pixels of the normalized

autocorrelations (values greater than 0.75, i.e. 3dB) of the ULM density images obtained respectively by the SVD-based algorithm (considered as a reference) and the proposed RPCA-based method. The calculated RG is 1.16, indicating a 16% improvement in the resolution of the proposed method over the SVD-based algorithm. The second one is contrast ratio (CR), a quantitative measure of contrast between the background and blood regions. A larger CR value indicates a better performance of ULM. For a pair of background and foreground patches, CR is defined as [17]:

$$\mathrm{CR}_{[\mathrm{dB}]} = 20 \log 10 \left(\frac{\mu_{\mathrm{R}_2}}{\mu_{\mathrm{R}_1}} \right),$$

where μ_{R_1} is the mean value of intensities in the blue rectangular patch R_1 which is kept fixed as a reference patch. μ_{R_2} is the mean value of intensities in the green rectangular patch R_2 which is one of the non-overlapping patches of the image (see Fig. 1). Fig. 2 shows the boxplot of all the patchwise CR values of the two algorithms. One can see that the proposed method results in a much better contrast, producing a much higher median value (46.11 for the proposed PRCA-based ULM and 23.45 for the SVD-based ULM). It proves the consistency with the above qualitative observation about the ULM density image results of the two studied techniques.

V. CONCLUSIONS

In this paper, we introduced an efficient algorithm of ultrafast ultrasound localization microscopy (ULM) for hemodynamic maps of the brain microvasculature, based on improving the tissue filtering performance using the robust principal component analysis (RPCA)-based method. The proposed method enabled more accurate ULM results than the reference method. Assessments carried out on *in vivo* rat brain perfusion dataset showed the benefits of using the proposed algorithm. Future work could be devoted, for instance, to deep learning (DL) techniques for automatic hyperparameter tuning, alleviating a practical downside of current state-of-the-art methods.

REFERENCES

[1] M. Tanter and M. Fink, "Ultrafast imaging in biomedical ultrasound," *IEEE Trans. Ultrason., Ferroelect., Freq. Control*, vol. 61, no. 1, pp. 102–119, Jan. 2014. DOI: 10.1109/TUFFC.2014.2882.

[2] O. Couture *et al.*, "Ultrasound Localization Microscopy and Super-Resolution: A State of the Art," *Ultrafast imaging in biomedical ultrasound*, vol. 65, no. 8, pp. 1304–1320, Aug. 2018. DOI: 10.1109/TUFFC.2018.2850811.

[3] C. Demené *et al.*, "Transcranial ultrafast ultrasound localization microscopy of brain vasculature in patients," *Nat. Biomed. Eng.*, vol. 5, no. 3, pp. 219–228, Mar. 2021. DOI: 10.1038/s41551-021-00697-x.

[4] K. Christensen-Jeffries *et al.*, "Super-resolution Ultrasound Imaging," *Ultrasound in Medicine & Biology*, vol. 46, no. 4, pp. 865–891, Apr. 2020. DOI: 10.1016/j.ultrasmedbio.2019.11.013.

[5] B. Heiles *et al.*, "Performance benchmarking of microbubble-localization algorithms for ultrasound localization microscopy," en, *Nat. Biomed. Eng*, vol. 6, no. 5, pp. 605–616, May 2022. DOI: 10.1038/s41551-021-00824-8.

[6] C. Demené *et al.*, "Spatiotemporal Clutter Filtering of Ultrafast Ultrasound Data Highly Increases Doppler and fUltrasound Sensitivity," *IEEE Trans. Med. Imaging*, vol. 34, no. 11, pp. 2271–2285, Nov. 2015. DOI: 10.1109/TMI.2015.2428634.

[7] E. J. Candès *et al.*, "Robust principal component analysis?" *Journal of the ACM*, vol. 58, no. 3, pp. 1–37, May 2011, Publisher: Association for Computing Machinery (ACM). DOI: 10.1145/1970392.1970395.

[8] S. Boyd *et al.*, "Distributed optimization and statistical learning via the alternating direction method of multipliers," *Found. Trends Mach. Learn.*, vol. 3, no. 1, pp. 1–122, 2010. DOI: 10.1561/2200000016.

[9] J. Wright *et al.*, "Robust Principal Component Analysis: Exact Recovery of Corrupted Low-Rank Matrices via Convex Optimization," in *Adv. Neural Inf. Process Syst.*, vol. 22, Curran Associates, Inc., 2009.

[10] Z. Lin *et al.*, "The augmented lagrange multiplier method for exact recovery of corrupted low-rank matrices," *Dept. Electr. Comput. Eng., UIUC, Urbana, Tech. Rep.*, 2009.

[11] J.-F. Cai *et al.*, "A Singular Value Thresholding Algorithm for Matrix Completion," *SIAM J. Optim.*, vol. 20, no. 4, pp. 1956–1982, Jan. 2010. DOI: 10.1137/080738970.

[12] D. H. Pham *et al.*, "Joint Blind Deconvolution and Robust Principal Component Analysis for Blood Flow Estimation in Medical Ultrasound Imaging," *IEEE Trans. Ultrason., Ferroelect., Freq. Control*, vol. 68, no. 4, pp. 969–978, 2020. DOI: 10.1109/TUFFC.2020.3027956.

[13] D. H. Pham *et al.*, "Fast High Resolution Blood Flow Estimation and Clutter Rejection Via an Alternating Optimization Problem," in *Proc. IEEE 18th (ISBI)*, 2021, pp. 1907–1910. DOI: 10.1109/ISBI48211.2021.9433816.

[14] R. Mcgill *et al.*, "Variations of Box Plots," *The American Statistician*, vol. 32, no. 1, pp. 12–16, Feb. 1978. DOI: 10.1080/00031305.1978.10479236.

[15] C. Arthur *et al.*, *OPULM PALA*, Type: dataset, Dec. 2020. DOI: 10.5281/ZENODO.4343435.

[16] Chengpu Yu *et al.*, "A blind deconvolution approach to ultrasound imaging," *IEEE Trans. Ultrason., Ferroelect., Freq. Control*, vol. 59, no. 2, pp. 271–280, Feb. 2012. DOI: 10.1109/TUFFC.2012.2187.

[17] A. Rodriguez-Molares *et al.*, "The Generalized Contrast-to-Noise Ratio," in *Proc. IEEE Int. Ultrason. Symp. (IUS)*, IEEE, Oct. 2018. DOI: 10.1109/ULTSYM.2018.8580101.